J|A|C|S
ARTICLES
Published on Web 10/05/2005

Electronic Relaxation Dynamics of Water Cluster Anions

Arthur E. Bragg,[†] Jan R. R. Verlet,[†] Aster Kammrath,[†] Ori Cheshnovsky,[‡] and Daniel M. Neumark*[,†,§]

Contribution from the Department of Chemistry, University of California, Berkeley, California 94720, School of Chemistry, The Sackler Faculty of Exact Sciences, Tel-Aviv University, 69978 Israel, and Chemical Sciences Division, Lawrence Berkeley National Laboratory, Berkeley, California 94720

Received April 29, 2005; E-mail: dneumark@berkeley.edu

Abstract: The electronic relaxation dynamics of water cluster anions, $(H_2O)_n^-$, have been studied with time-resolved photoelectron imaging. In this investigation, the excess electron was excited through the $p \leftarrow s$ transition with an ultrafast laser pulse, with subsequent electronic evolution monitored by photodetachment. All excited-state lifetimes exhibit a significant isotope effect ($\tau_{D_2O}/\tau_{H_2O} \sim 2$). Additionally, marked dynamical differences are found for two classes of water cluster anions, isomers I and II, previously assigned as clusters with internally solvated and surface-bound electrons, respectively. Isomer I clusters with $n \geq 25$ decay exclusively by internal conversion, with relaxation times that extrapolate linearly with $1/n$ toward an internal conversion lifetime of 50 fs in bulk water. Smaller isomer I clusters ($13 \leq n \leq 25$) decay through a combination of excited-state autodetachment and internal conversion. The relaxation of isomer II clusters shows no significant size dependence over the range of $n = 60-100$, with autodetachment an important decay channel following excitation of these clusters. Photoelectron angular distributions (PADs) were measured for isomer I and isomer II clusters. The large differences in dynamical trends, relaxation mechanisms, and PADs between large isomer I and isomer II clusters are consistent with their assignment to very different electron binding motifs.

1. Introduction

The hydrated electron (e_{aq}^-) has captured the attention of physical scientists throughout the last half-century.[1,2] This species has been recognized as an important participant in radiation chemistry and as an important reagent in charge-induced reactivity, molecular-biological processes, and condensed-phase chemistry. The significance of e_{aq}^- has sparked much experimental activity aimed at characterizing its energetics and dynamics in solution through various spectroscopic methods.[3−13] Additionally, this species stands as a most fundamental quantum-mechanical solute, such that modeling its properties through various theoretical approaches provides new insights into condensed-phase dynamics.[14−19] Simulations have also been crucial to assigning experimental signatures of this species at equilibrium and in transient states.[20,21] For instance, simulations have helped establish that the equilibrated hydrated electron has an *s*-like wave function and is supported within a cavity of ~6 water molecules. They have also demonstrated that the absorption spectrum of the hydrated electron arises from a nominal $p \leftarrow s$ transition within the solvent cavity. While the assignment of the spectrum is largely (but not univerally[22]) accepted, interpretation of hydrated-electron dynamics remains controversial.[7,12,16] Studies of water cluster anions, $(H_2O)_n^-$, offer a parallel approach to understanding essential features of electron hydration by probing in detail the size-dependent photophysical properties of these clusters.[23−31] In this contribution, we present

[†] University of California.
[‡] Tel-Aviv University.
[§] Lawrence Berkeley National Laboratory.

(1) Hart, E. J.; Boag, J. W. *J. Am. Chem. Soc.* **1962**, *84*, 4090.
(2) Boag, J. W.; Hart, E. J. *Nature* **1963**, *197*, 45.
(3) Wiesenfeld, J. M.; Ippen, E. P. *Chem. Phys. Lett.* **1980**, *73*, 47.
(4) Migus, A.; Gauduel, Y.; Martin, J. L.; Antonetti, A. *Phys. Rev. Lett.* **1987**, *58*, 1559.
(5) Shi, X. L.; Long, F. H.; Lu, H.; Eisenthal, K. B. *J. Phys. Chem.* **1996**, *100*, 11903.
(6) Hertwig, A.; Hippler, H.; Unterreiner, A. N.; Vöhringer, P. *Ber. Bunsen-Ges. Phys. Chem.* **1998**, *102*, 805.
(7) Yokoyama, K.; Silva, C.; Son, D. H.; Walhout, P. K.; Barbara, P. F. *J. Phys. Chem. A* **1998**, *102*, 6957.
(8) Assel, M.; Laenen, R.; Laubereau, A. *J. Phys. Chem. A* **1998**, *102*, 2256.
(9) Assel, M.; Laenen, R.; Laubereau, A. *Chem. Phys. Lett.* **2000**, *317*, 13.
(10) Son, D. H.; Kambhampati, P.; Kee, T. W.; Barbara, P. F. *J. Phys. Chem. A* **2001**, *105*, 8269.
(11) Tauber, M. J.; Mathies, R. A. *J. Am. Chem. Soc.* **2003**, *125*, 1394.
(12) Pshenichnikov, M. S.; Baltuska, A.; Wiersma, D. A. *Chem. Phys. Lett.* **2004**, *389*, 171.
(13) Lee, Y. J.; Kee, T. W.; Zhang, T. Q.; Barbara, P. F. *J. Phys. Chem. B* **2004**, *108*, 3474.
(14) Rossky, P. J.; Schnitker, J. *J. Phys. Chem.* **1988**, *92*, 4277.
(15) Neria, E.; Nitzan, A.; Barnett, R. N.; Landman, U. *Phys. Rev. Lett.* **1991**, *67*, 1011.
(16) Schwartz, B. J.; Rossky, P. J. *J. Chem. Phys.* **1994**, *101*, 6902.
(17) Schwartz, B. J.; Rossky, P. J. *J. Chem. Phys.* **1994**, *101*, 6917.
(18) Rips, I. *Chem. Phys. Lett.* **1995**, *245*, 79.
(19) Bratos, S.; Leicknam, J. C.; Borgis, D.; Staib, A. *Phys. Rev. E* **1997**, *55*, 7217.
(20) Schnitker, J.; Motakabbir, K.; Rossky, P. J.; Friesner, R. *Phys. Rev. Lett.* **1988**, *60*, 456.
(21) Boero, M.; Parrinello, M.; Terakura, K.; Ikeshoji, T.; Liew, C. C. *Phys. Rev. Lett.* **2003**, *9022*, 6403.
(22) Sobolewski, A. L.; Domcke, W. *Phys. Chem. Chem. Phys.* **2002**, *4*, 4.
(23) Haberland, H.; Ludewight, C.; Schindler, H. G.; Worsnop, D. R. *J. Chem. Phys.* **1984**, *81*, 3742.
(24) Haberland, H.; Ludewight, C.; Schindler, H. G.; Worsnop, D. R. *Surf. Sci.* **1985**, *156*, 157.

a comprehensive picture of size-, isotopomer-, and isomer-dependent electronic relaxation dynamics in $(H_2O)_n^-/(D_2O)_n^-$ that yields considerable insight into the nature of these finite-sized species and their relation to e_{aq}^-.

The photoelectron (PE),[25,30,32] electronic absorption,[26,27] and vibrational absorption[28,29] spectra of water cluster anions have been investigated in order to assess whether and at what size these clusters possess the characteristics of e_{aq}^-. Interpretation of these experiments has been facilitated by many theoretical studies of these anions using quantum path integral, molecular dynamics (MD), and electronic structure methods.[33−42] In the first investigation of these species with PE spectroscopy, Bowen and co-workers[25] demonstrated that the size-dependent vertical binding energies (VBEs) of clusters $n = 6, 7, 11-69$ extrapolate to a sensible, but unmeasured, bulk photoelectric threshold (PET) value according to an electrostatic model ($[\mathrm{VBE}(n) - \mathrm{PET}] \propto n^{-1/3} \propto 1/R$). The size dependence of measured VBEs were recovered from this model using only the dielectric constants of bulk water. While the PET of the bulk-hydrated electron has not been measured directly, the size-dependent VBEs of the analogous $(NH_3)_n^-$ ($n = 41-1100$) clusters, which are anticipated to host the excess electron internally, extrapolate sensibly to the measured PET of the bulk-ammoniated electron.[43] This set of observations led Bowen to assign the observed water cluster anions to structures with internally solvated electrons. Ayotte and Johnson[26] found that electron absorption maxima of $(H_2O)_n^-$ ($n = 6-50$) likewise extrapolate to the absorption maximum of the bulk-hydrated electron. However, the measured VBEs and absorption maxima also matched those of surface-bound electrons, as calculated by Barnett et al.,[34] fueling much debate about the true nature of the excess electron in clusters of this size regime, as no other isomers were observed at these larger ($n > 11$) sizes, and thus raising questions regarding their similarity to e_{aq}^-.

Two recently reported spectroscopic studies of $(H_2O)_n^-$ offer fresh perspective regarding the nature of the excess electrons in these clusters. Through comparison of measured vibrational spectra to those anticipated for various calculated cluster geometries, Hammer et al.[29] have assigned a binding motif to the isomer of small water cluster anions ($n = 4-6$) with the most highly bound electron. Specifically, these authors demonstrated that the excess electron is bound by a "double-acceptor" water molecule, with both H atoms oriented toward the electron, and the collective dipole of the water network.

In our group, three general classes of large ($n > 11$) water cluster anion isomers were recently identified according to their size-dependent VBEs; these isomer classes were observed through manipulation of cluster-ion source conditions.[30] The VBEs for the class of isomers with the most tightly bound electrons, isomer I, agreed with the values found by Bowen.[25] Two additional broad classes of cluster isomers with considerably lower VBEs, isomer II and the less prevalent isomer III, had not been observed in this size regime prior to our work. Based on expectations from theory[34] that internally solvated electrons should be bound more strongly than those on the surface, a trend that has been supported in more recent papers as well,[42,44] isomer I was assigned to water clusters with internally solvated electrons (in agreement with Bowen), while isomers II and III were assigned as surface-bound species. These assignments were supported by trends in the excited-state lifetimes,[30,45] which are strongly dependent on size for isomer I clusters but virtually size-independent for isomer II clusters.

The "cluster approach" has also motivated a series of experiments[27,45,46] aimed at probing the time-resolved electronic relaxation dynamics of $(H_2O)_n^-$, with the goal of elucidating the relaxation mechanism of the bulk-hydrated electron. In a femtosecond resonant two-photon detachment (fs-R2PD) study, Weber et al.[27] estimated an upper limit of 150 fs for the excited state in clusters ranging in size from 20 to 100 water molecules. In our group, the time scales for $p \rightarrow s$ decay in $(H_2O)_n^-/(D_2O)_n^-$ ($n = 25-50$) were measured using two-color time-resolved photoelectron imaging (TRPEI).[45] Our observation of rapid relaxation lifetimes, a significant dynamical isotope effect ($\tau_{D_2O}/\tau_{H_2O} \sim 2$), an absence of observable excited-state solvation dynamics, and the extrapolation of cluster lifetimes to ultrafast decay time scales (50 and 70 fs for $(H_2O)_n^-$ and $(D_2O)_n^-$, respectively) in bulk water are consistent with the "nonadiabatic" relaxation mechanism of the hydrated electron.[12,47] According to this proposed condensed-phase relaxation mechanism, $p \rightarrow s$ internal conversion (IC) occurs on a 50-fs (70-fs) time scale in bulk H_2O (D_2O) and is followed by a two-step ground-state relaxation process exhibiting a considerably weaker isotopic effect. Alternative models, "adiabatic" relaxation mechanisms, were developed from mixed quantum-classical MD simulations of hydrated-electron dynamics;[16] these models involve a much slower internal conversion rate, preceded by excited-state relaxation dynamics.

In a complementary study, Paik et al.[46] used time-resolved photoelectron spectroscopy to probe the ground-state relaxation dynamics in $(H_2O)_n^-$ ($n = 15-35$) after internal conversion. Their results closely match the longer time scales measured in transient absorption experiments conducted with the bulk-hydrated system. These findings are likewise consistent with the nonadiabatic relaxation model and suggest that the essential

(25) Coe, J. V.; Lee, G. H.; Eaton, J. G.; Arnold, S. T.; Sarkas, H. W.; Bowen, K. H.; Ludewigt, C.; Haberland, H.; Worsnop, D. R. *J. Chem. Phys.* **1990**, *92*, 3980.
(26) Ayotte, P.; Johnson, M. A. *J. Chem. Phys.* **1997**, *106*, 811.
(27) Weber, J. M.; Kim, J.; Woronowicz, E. A.; Weddle, G. H.; Becker, I.; Cheshnovsky, O.; Johnson, M. A. *Chem. Phys. Lett.* **2001**, *339*, 337.
(28) Ayotte, P.; Weddle, G. H.; Bailey, C. G.; Johnson, M. A.; Vila, F.; Jordan, K. D. *J. Chem. Phys.* **1999**, *110*, 6268.
(29) Hammer, N. I.; Shin, J. W.; Headrick, J. M.; Diken, E. G.; Roscioli, J. R.; Weddle, G. H.; Johnson, M. A. *Science* **2004**, *306*, 675.
(30) Verlet, J. R. R.; Bragg, A. E.; Kammrath, A.; Cheshnovsky, O.; Neumark, D. M. *Science* **2005**, *307*, 93.
(31) Coe, J. V., *Int. Rev. Phys. Chem.* **2001**, *20*, 33.
(32) Kim, J.; Becker, I.; Cheshnovsky, O.; Johnson, M. A. *Chem. Phys. Lett.* **1998**, *297*, 90.
(33) Barnett, R. N.; Landman, U.; Cleveland, C. L.; Jortner, J. *Phys. Rev. Lett.* **1987**, *59*, 811.
(34) Barnett, R. N.; Landman, U.; Cleveland, C. L.; Jortner, J. *J. Chem. Phys.* **1988**, *88*, 4429.
(35) Barnett, R. N.; Landman, U.; Nitzan, A. *J. Chem. Phys.* **1989**, *91*, 5567.
(36) Kim, K. S.; Park, I.; Lee, S.; Cho, K.; Lee, J. Y.; Kim, J.; Joannopoulos, J. D. *Phys. Rev. Lett.* **1996**, *76*, 956.
(37) Lee, S.; Kim, J.; Lee, S. J.; Kim, K. S. *Phys. Rev. Lett.* **1997**, *79*, 2038.
(38) Jordan, K. D.; Wang, F. *Annu. Rev. Phys. Chem.* **2003**, *54*, 367.
(39) Jordan, K. D. *Science* **2004**, *306*, 618.
(40) Khan, A. *J. Chem. Phys.* **2004**, *121*, 280.
(41) Lee, H. M.; Suh, S. B.; Tarakeshwar, P.; Kim, K. S. *J. Chem. Phys.* **2005**, *122*, 044309.
(42) Herbert, J. M.; Head-Gordon, M. *J. Phys. Chem. A* **2005**, *109*, 5217.
(43) Sarkas, H. W.; Arnold, S. T.; Eaton, J. G.; Lee, G. H.; Bowen, K. H. *J. Chem. Phys.* **2002**, *116*, 5731.
(44) Khan, A. *J. Chem. Phys.* **2003**, *118*, 1684.
(45) Bragg, A. E.; Verlet, J. R. R.; Kammrath, A.; Cheshnovsky, O.; Neumark, D. M. *Science* **2004**, *306*, 669.
(46) Paik, D. H.; Lee, I.-R.; Yang, D.-S.; Baskin, J. S.; Zewail, A. H. *Science* **2004**, *306*, 672.
(47) Kimura, Y.; Alfano, J. C.; Walhout, P. K.; Barbara, P. F. *J. Phys. Chem.* **1994**, *98*, 3450.

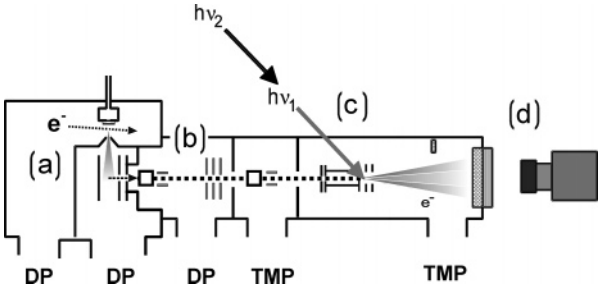

Figure 1. Time-resolved photoelectron imaging apparatus: (a) ion source region; (b) time-of-flight (TOF) mass spectrometer; (c) laser interaction region and ion-beam collinear velocity-map imaging (VMI) lens; (d) photoelectron imaging system. DP = diffusion pump, TMP = turbomolecular pump. Arrows (labeled $h\nu_1$ and $h\nu_2$) indicate femtosecond pump and probe laser pulses.

dynamical features of e_{aq}^- may be present at relatively small cluster sizes ($n \approx 25$). However, a firm understanding of how the bulk and cluster environments are related, and at what size they are analogous, is still lacking.

In this paper, we present photoelectron images and time-resolved dynamics over an expanded range of cluster sizes in order to gain further insight into water cluster anions and their connection with e_{aq}^-. Specifically, we describe the electronic relaxation dynamics of $(H_2O)_{n,I}^-/(D_2O)_{n,I}^-$ ($n = 13-100$) and $(H_2O)_{n,II}^-/(D_2O)_{n,II}^-$ ($n = 60-100$), where "I" and "II" denote the isomers broadly assigned to clusters with "internalizing"/internally solvated and localized surface-solvated electrons, respectively. We find that the relaxation dynamics of electrons in $(H_2O)_{n,I}^-$ are dominated by internal conversion for clusters with $n \geq 25$, for which the lifetime scales as $1/n$. An abrupt change in this trend is seen for smaller isomer I clusters and is attributed to a competing excited-state autodetachment decay channel. The dynamics of $(H_2O)_{n,II}^-$ are highlighted by similar competing excited-state dynamics and a similar isotopic effect ($\sim$2) as small $(H_2O)_{n,I}^-$, but with relaxation occurring over longer time scales and with no apparent size dependence. Excited-state autodetachment appears to be significantly more important as a decay mechanism in the isomer II clusters, consistent with their assignment as clusters with surface-bound electrons. We present photoelectron angular distributions (PADs) measured from the ground and excited states of these isomers; trends in PAD anisotropies with size and isomer offer insight into the nature of the orbital shapes of the excess electron in these clusters. We close with a discussion of the implications of these results with regard to the nature of the excess electron in these clusters and the connection between the cluster and bulk experiments.

2. Experimental Section

A diagram of our apparatus is given in Figure 1. The techniques used in this study are well-documented in previous publications.[48−50] Briefly, water-cluster anions are generated with a pulsed source in region (a),[51] mass-separated by time-of-flight in region (b), and photoexcited and photodetached by femtosecond laser pulses. The resulting photoelectrons are collected and analyzed with a collinear velocity-map imaging[52] system comprising electron optics (c) and a detector/camera (d), yielding the electron kinetic energy (*eKE*) and photoelectron angular distributions (PADs).

Our apparatus is based on general pulsed-ion techniques developed by Lineberger and co-workers.[51] Water-cluster anions were generated in region (a) by passing 30−70 psig of Ar over H_2O/D_2O prior to supersonic expansion into a vacuum through a High-Temperature Even−Lavie pulsed valve[53] at a 100-Hz repetition rate. The neutral beam produced subsequently intersects a pulsed electron beam, which generates cations and anions through collisional detachment and secondary electron attachment, respectively.[51] $(H_2O)_{n,I}^-$ clusters were generated at source backing pressures of 30−40 psi, whereas $(H_2O)_{n,II}^-$ clusters were formed at higher backing pressure ($\sim$70 psi), as described previously.[30] Anions in the beam are injected into a Wiley−McLaren time-of-flight mass spectrometer[54] [region (b)] with an average kinetic energy of $\sim$1800 eV. The isotopic purity of these clusters was readily assessed based on the relative quantities of OD^- and OH^- observed in the ion beam. Water clusters were generated from distilled H_2O, whereas perdeutero water clusters were produced with D_2O (99.9% purity) obtained from Cambridge Isotope.

Photoelectrons were collected using collinear anion velocity-map imaging (VMI). Our implementation of this technique has been documented extensively elsewhere[48] and is similar to that used by Sanov[55] and Bordas,[56] with the difference that photoelectrons are extracted collinearly, rather than perpendicularly, with respect to the parent ion beam. The ion packet of interest is first isolated and introduced into the laser interaction region by briefly lowering an HV potential gate, which behaves as a mass gate in the time-of-flight mass spectrometer. This potential is also applied to an ion re-referencing tube located beyond the mass gate, as well as to the VMI repeller electrode. The VMI electron optical stack, based on the original design of Eppink and Parker,[52] is composed of three electrodes, repeller, extractor, and ground, that provide the cylindrically symmetric non-homogeneous electric field required to produce a charged-particle immersion lens. Three-dimensional photoelectron distributions generated in the laser interaction region, between the repeller and extractor electrodes, are accelerated and mapped onto a microchannel plate (MCP) detector coupled to a CCD camera. Optimal image focusing is obtained using a 70% extractor/repeller potential ratio, with typical absolute extractor/repeller voltages ranging from 1400 V/2000 V to 2800 V/4000 V; absolute voltages were chosen in accord with a desired degree of image magnification. Importantly, cluster binding energies and relaxation lifetimes measured were not affected by the imaging field strength ($<\sim$100 V/mm).

A pulsed "gain gate" applied to the MCP stack limits signal amplification to the electron arrival time, thereby reducing background and eliminating ion signal collection. Phosphor emission is imaged with a Dalsa-1M30 CCD camera (Uniforce) at a 50-Hz repetition rate, such that each frame captures electrons generated from two consecutive laser shots. The camera collects images in a 2×2 pixel binning mode (effectively, 512×512 pixels) in order to increase camera frequency and overall collection speed.

Pump and probe frequencies used in this experiment were generated from the 790 nm (1.57 eV), 1 mJ (500 Hz), 80 fs fwhm chirped-pulse amplified output of a Ti:Sapphire femtosecond oscillator (Clark-MXR NJA-5, CPA-1000) through various frequency conversion schemes. Near infrared (NIR) excitation wavelengths (790, 1250, and 1650 nm), provided by the 790 nm laser fundamental or a fundamental-pumped optical parametric amplifier (OPA) (TOPAS, Light Conversion), were

(48) Bragg, A. E.; Verlet, J. R. R.; Kammrath, A.; Neumark, D. M. *J. Chem. Phys.* **2004**, *121*, 3515.
(49) Bragg, A. E.; Wester, R.; Davis, A. V.; Kammrath, A.; Neumark, D. M. *Chem. Phys. Lett.* **2003**, *376*, 767.
(50) Davis, A. V.; Wester, R.; Bragg, A. E.; Neumark, D. M. *J. Chem. Phys.* **2003**, *118*, 999.
(51) Johnson, M. A.; Lineberger, W. C. Pulsed methods for cluster ion spectroscopy. In *Techniques of Chemistry*; Farrar, J. M., Saunders, W. H., Jr., Eds.; Wiley Journal: New York, 1988; Vol. 20, pp 591−635.
(52) Eppink, A. T. J. B.; Parker, D. H. *Rev. Sci. Instrum.* **1997**, *68*, 3477.
(53) Even, U.; Jortner, J.; Noy, D.; Lavie, N.; Cossart-Magos, C. *J. Chem. Phys.* **2000**, *112*, 8068.
(54) Wiley, W. C.; McLaren, I. H. *Rev. Sci. Instrum.* **1955**, *26*, 1150.
(55) Surber, E.; Sanov, A. *J. Chem. Phys.* **2002**, *116*, 5921.
(56) Bordas, C.; Paulig, F.; Helm, H.; Huestis, D. L. *Rev. Sci. Instrum.* **1996**, *67*, 2257.

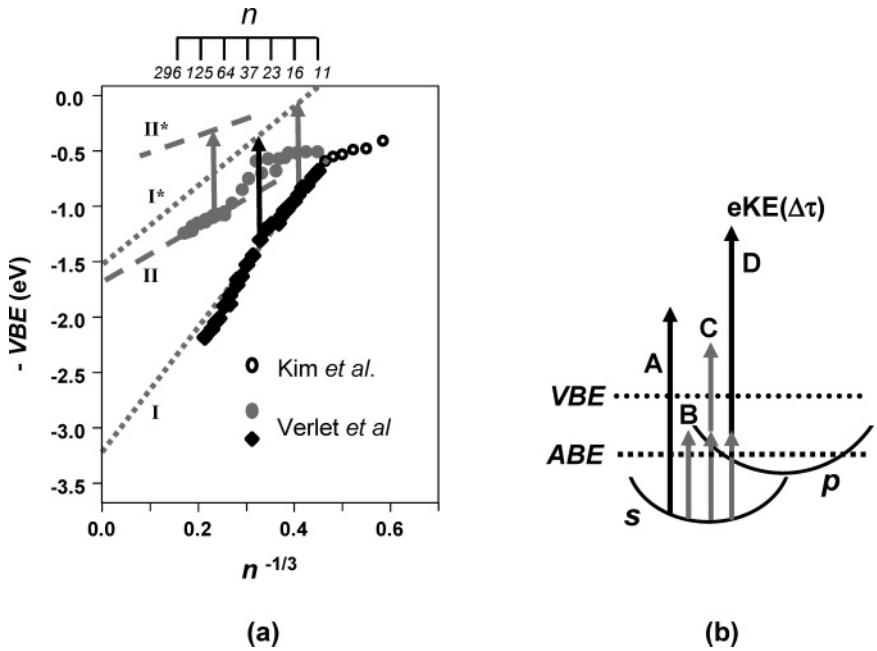

Figure 2. (a) Size- and isomer-dependent level energetics of water cluster anions: (filled diamonds and circles) isomer I and II vertical binding energies (VBEs, ref 30), respectively; (empty circles) small cluster VBEs (ref 32). (Dotted and dashed lines) excited states of isomer I and II $(H_2O)_n^-$ (I* and II*, respectively) determined from refs 26 and 57, respectively. Arrows indicate excitation energies (0.75 eV, gray, and 1.0 eV, black) used in time-resolved studies reported here. (b) Electronic level energetics of $(H_2O)_n^-$ are characterized by a bound *s*-like ground state and three nearly-degenerate bound *p*-like excited states below the VBE. Pump−probe photodetachment images/spectra have contributions from (A) above-VBE detachment at the probe laser energy; (B) above-ABE (adiabatic binding energy) photodetachment at the pump laser energy; (C) resonant two-photon detachment (R2PD) at the pump energy; (D) resonant, time-dependent, two-color, two-photon pump−probe detachment signal.

selected according to the known[26] and calculated[57] absorption maxima of each investigated size regime and isomer and to minimize direct pump-induced photodetachment. Dynamics were probed through photodetachment with the 790-nm fundamental or 395-nm light produced by second harmonic generation of the fundamental. The excitation and photodetachment energies were routinely measured with an Ocean Optics spectrometer, following frequency conversion (SHG or SFG) to a visible wavelength in the case of NIR wavelengths. The temporal cross-correlation of the pump and probe pulses was typically ∼130−150 fs and was measured through frequency mixing in various nonlinear optical crystals. Photodetachment spectra collected with various VMI fields were calibrated to the photodetachment spectrum of O^- collected at 395 nm. The IR pump pulse was delayed with respect to the fixed UV optical path length through use of a computer-controlled translation stage. A 50-cm lens focused the collinearly-recombined beams within the interaction region of the VMI lens.

Data were typically acquired for 10 000−20 000 laser shots (100−200 s) at each pump−probe delay, generally resulting in the collection of $\sim 10^5-10^6$ photoelectrons at each delay. Photoelectron spectra were normalized according to the integrated probe-only signal (395 or 790 nm direct photodetachment), collected between pump−probe images, to compensate for fluctuations in ion intensity with collection time. All images have been four-way symmetrized in order to account for nonhomogeneous detector and CCD sensitivity. Three-dimensional velocity distributions collected in time-resolved experiments were reconstructed using the Basis Set Expansion (BASEX) forward convolution method developed by Dribinski et al.[58] Photoelectron kinetic energy distributions were obtained through velocity→energy transformation and radial integration of the $\phi = 0$ slice of reconstructed, cylindrically symmetric 3D detachment distributions. The kinetic energy resolution, $\Delta E/E$, is ∼5% following atomic anion photodetachment. Photoelectron angular distribution anisotropy parameters, $\beta_n(\epsilon)$, are acquired by fitting the 3D slice with an even series of associated Legendre polynomials ($P_n(\cos\theta)$) appropriately truncated for an *m*-photon photodetachment process ($n_{max} = 2m$).[59] We applied the pBASEX method, recently developed by Garcia et al.,[60] to reconstruct PADs with high fidelity to determine $\beta_n(\epsilon)$'s; details are discussed in the Analysis.

3. Results

Size-dependent VBEs of isomer I and II clusters are summarized in Figure 2a for $n = 11-200$; open circles, representing the high-VBE isomer observed at sizes $n < 11$, were taken from the measurements of Kim et al.[32] Isomer II clusters were observed throughout this range with D_2O, but only at sizes $n > 27$ with H_2O. A third, more weakly bound class of anions (isomer III) was discovered and reported previously;[30] this isomer is not shown in Figure 2a and is not considered further in this paper.

The trends in Figure 2a reflect the ground-state energetics of the cluster isomers with size and indicate the divergence of isomer-dependent VBEs at $n = 11$. The VBEs of isomer I follow the $n^{-1/3}$ dependence noted by Coe et al.[25] (dashed line). VBEs of the more weakly bound $(H_2O)_{n,II}^-$ clusters extrapolate well at $n < 20$ to those of small clusters ($n < 11$) investigated by Kim et al.,[32] exhibit considerable nonlinear evolution between 20 and 50 water molecules, and reflect a new regime of linearity at sizes $n > 50$. The cluster sizes accessible to time-resolved experiments were limited by the ability to isolate the isomer of interest through manipulation of the cluster-ion source conditions. Consequently, while an extended size range of isomer I was available for investigation, only larger ($n = 60-100$) isomer II clusters could be studied in time-resolved experiments, as

(57) Barnett, R. N.; Landman, U.; Makov, G.; Nitzan, A. *J. Chem. Phys.* **1990**, *93*, 6226.
(58) Dribinski, V.; Ossadtchi, A.; Mandelshtam, V. A.; Reisler, H. *Rev. Sci. Instrum.* **2002**, *73*.
(59) Reid, K. L. *Annu. Rev. Phys. Chem.* **2003**, *54*, 397.
(60) Garcia, G.; Nahon, L.; Powis, I. *Rev. Sci. Instrum.* **2004**, *75*, 4989.

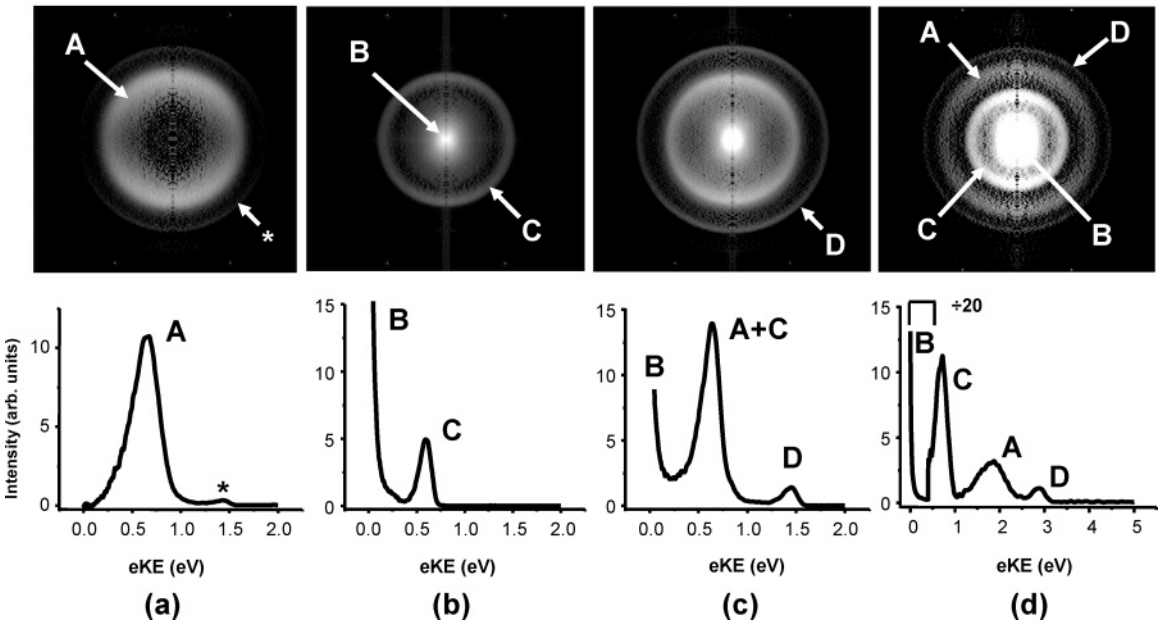

Figure 3. (a−c) Photoelectron images (inverted) and spectra of isomer I $(D_2O)_{15}^-$ [$(D_2O)_{15,I}^-$]: (a) 790 nm only (* marks an additional isomer of $(D_2O)_{15}^-$ observed previously at these size ranges); (b) 1650 nm only; (c) 1650 nm + 790 nm pump−probe at $t = 0$. (d) 1250 nm + 395 nm pump−probe of $(D_2O)_{25,I}^-$ at $t = 0$. All photodetachment features are assigned to the processes presented in Figure 2b.

both isomers are generated in high yield at small cluster sizes even at large source backing pressures.

Despite an anticipated difference in the local solvation environment of electrons supported by these two isomers, calculations characterize both internally localized and surface-localized electrons with the same general electronic level structure,[57] outlined in Figure 2b. This electronic level scheme is similar to that of e_{aq}^-[14] and that recently calculated for an electron localized at a bulk water−air interface.[61] Both species possess bound, localized *s*-like and degenerate *p*-like electronic states, with the exception that the detachment continuum [$(H_2O)_n + e^-$] replaces the conduction band of water in $(H_2O)_n^-$. The size-dependent excited-state (*p*) energetics of each isomer are plotted in Figure 2a as the $p \leftarrow s$ absorption maximum referenced to the cluster VBE, where the former has been determined by experiment[26] (I*, dotted) or has been taken from calculations[57] (II*, dashed), with the latter association based on our previous assignment of isomer II to a general species with surface-bound electrons.

Photoexcitation wavelengths used here were selected in order to maximize absorption as well as to minimize the direct pump-induced photodetachment near the adiabatic threshold. The specific probe wavelength applied in our time-resolved experiments at a given cluster size was determined by the cluster VBE, since population transfer between excited and ground states is best observed when the probe energy exceeds the VBE of the ground-state cluster. Large $(H_2O)_{n,I}^-$ were excited with either the 1250 nm (1.0 eV, 15−20 μJ/pulse) signal output of the OPA ($25 < n < 50$) or the 790 nm (1.57, 10−20 μJ/pulse) laser fundamental ($45 < n < 100$) and were probed subsequently through photodetachment at 395 nm (3.14 eV, 80−90 μJ, ∼100 fs). Small $(H_2O)_{n,I}^-$ ($13 < n < 28$) and the large $(H_2O)_{n,II}^-$ ($60 < n < 100$) were excited with the 1650 nm (0.75 eV, 30−40 μJ/pulse) idler output of the OPA and were subsequently probed through detachment at 790 nm (∼150 μJ/pulse). The dynamics of large isomer II clusters were additionally probed at 395 nm, sufficient to photodetach both isomer I and II clusters, in order to investigate the possibility of binding-mode isomerization following electronic excitation. The arrows in Figure 2a relate photoexcitation energies to the cluster size regimes of each isomer investigated here. Photoexcitation schemes relevant to these investigations are also shown in Figure 2b; detachment channels (lettered) and excitation/relaxation processes are explained below in context to our observations.

Representative one- and two-photon BASEX-transformed photodetachment images and PE spectra of $(D_2O)_{15,I}^-$ are presented in Figure 3a−c. In all images, larger radii correspond to higher electron velocities and, consequently, higher photoelectron kinetic energies. Figure 3a presents the image and spectrum obtained with 790 nm. The intense ring is seen in the image peaks at an *eKE* of 0.67 eV and results from one-photon detachment of the *s* electron (process A in Figure 2b). The weak feature at larger radii (marked with * and peaking at 1.43 eV) corresponds to the previously observed[30] isomer III of $(D_2O)_{15}^-$. Figure 3b shows the image and spectrum of the same cluster at 1650 nm. The spectrum is dominated by a low-*eKE* feature resulting from a combination of direct photodetachment from the *s* state and excited-state (*p* state) autodetachment [Figure 2b, process B], as the pump photon energy exceeds the adiabatic detachment threshold of this cluster. The higher energy feature peaking at $eKE = 0.61$ eV occurs by resonant two-photon detachment (R2PD, process C) through the excited state of the cluster; the presence of this feature highlights that 1650 nm is an appropriate pump wavelength for initiating excited-state dynamics at this cluster size.

Figure 3c displays features from temporally overlapped pump (1650 nm) and probe (790 nm) pulses. The large peak "A + C" at 0.6 eV arises from a combination of direct detachment at 790 nm and R2PD at 1650 nm, overlapping because $\lambda_{pu} \approx 2\lambda_{pr}$. The high-energy feature is from pump−probe excitation via the excited state (process D, Figure 2b) and is time-dependent, with

(61) Rodriguez, J.; Laria, D. *J. Phys. Chem. B* **2005**, *109*, 6473.

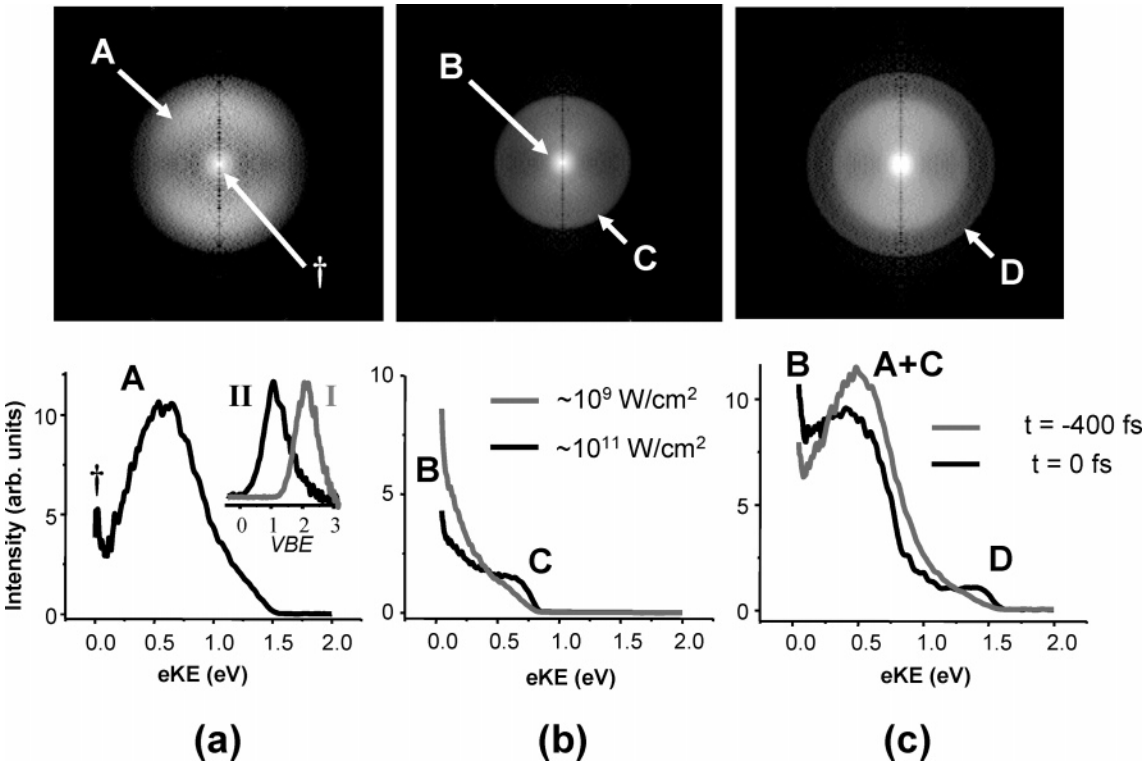

Figure 4. Photoelectron images (inverted) and spectra of isomer II $(D_2O)^-_{80}$ [$(D_2O)^-_{80,II}$]: (a) 790 nm only; † indicates threshold photodetachment of $(D_2O)^-_{80,I}$. The inset shows PE spectra of isomers I and II at 395 nm. (b) 1650 nm only; images have been collected at different laser fluences, indicating that feature C is from R2PD. (c) 1650 nm + 790 nm pump−probe at $t = 0$ fs (image and black spectrum); the spectrum in gray was collected outside of the temporal pulse overlap ($t = -400$ fs). All photodetachment features are assigned to the processes in Figure 2b.

its time-evolving intensity reflecting *p*-state decay dynamics. Figure 3d displays a similar two-color image and spectrum of the $(D_2O)^-_{25,I}$ cluster pumped and probed with photons of higher energy, with $E_{ex} = 1.0$ eV (1250 nm) and $E_{pr} = 3.14$ eV (395 nm). Here all detachment peaks seen in Figure 3a−c are observed clearly, as the 1.0 eV R2PD and 3.14 eV direct detachment signals do not overlap energetically, in contrast to the scenario presented in Figure 3c. While the intensity of feature D exhibits the strongest dependence on pump−probe delay, other features in the two-color spectra are also time-dependent as discussed below.

Figure 4 presents images and spectra for a typical large isomer II cluster, $(D_2O)^-_{80,II}$. Figure 4a and b show results for one-color photodetachment at 790 and 1650 nm, respectively, while Figure 4c gives two-color results. Figure 4a is dominated by direct detachment of isomer II (peak A), with a small contribution at very low *eKE* from residual quantities of isomer I; the inset of Figure 4a plots spectra from both $(D_2O)^-_{80,II}$ and $(D_2O)^-_{80,I}$ collected following 395 nm photodetachment and illustrates the disparate VBEs of these two isomers, as plotted in Figure 2a. Figure 4b shows a signal from direct detachment (B) and R2PD (C) via the excited state of the surface-bound electron; the relative intensity of feature C increases dramatically at higher laser power, as expected for a two-photon process. Finally, Figure 4c shows a time-dependent pump−probe feature D (λ_{pu} =1650 nm, λ_{pr} =790 nm) collected at $\Delta t = 0$; the gray PE spectrum shows that this feature is not present when the probe precedes the pump pulse. Evolution of this feature reflects the excited-state dynamics of this cluster.

Spectral "waterfall" plots highlighting the time dependence of various features in the two-color PE images and spectra are presented in Figure 5; results are presented for $(D_2O)^-_{15,I}$ (a), $(D_2O)^-_{25,I}$ (b), and $(D_2O)^-_{80,II}$ (c), while Figure 6 plots the integrated intensities of each labeled feature in Figure 5 for the three clusters. Only for $(D_2O)^-_{25,I}$ is feature C separable from feature A, as shown in Figure 5c. However, the absolute increase in C is considerably smaller than the recovery amplitude in A, indicating that the dynamic most responsible for evolution of feature "A + C" in Figures 5(a,b) is the recovery in the direct (probe) photodetachment signal.

In all cases, the dynamics are characterized by a cross-correlation-limited (∼130−150 fs) rise in the intensity of features D, C, and B, with a simultaneous pump-induced depletion in feature A. Subsequently, feature D decays and A partially recovers on a time scale outside of the temporal cross-correlation, while feature B remains constant (Figure 5b) or increases slightly (Figure 5a,c) with time. This overall rise or decay of each feature "X" = A, B, D is indicated by Δ"X" in Figure 6.

4. Analysis

4.1. Time-Resolved Relaxation Dynamics. Each temporal trace of the type shown in Figure 6 has been fitted to a single-exponential decay/recovery function convoluted with the temporal cross-correlation of the pump and probe laser pulses. All fitting functions (prior to convolution) have the general form

$$I(t) = A_0,\ t < 0$$

$$I(t) = A_1 + A_2 \exp(-t/\tau),\ t \geq 0 \qquad (1)$$

in which $A_{0,1}$ are constant signal offsets that account for

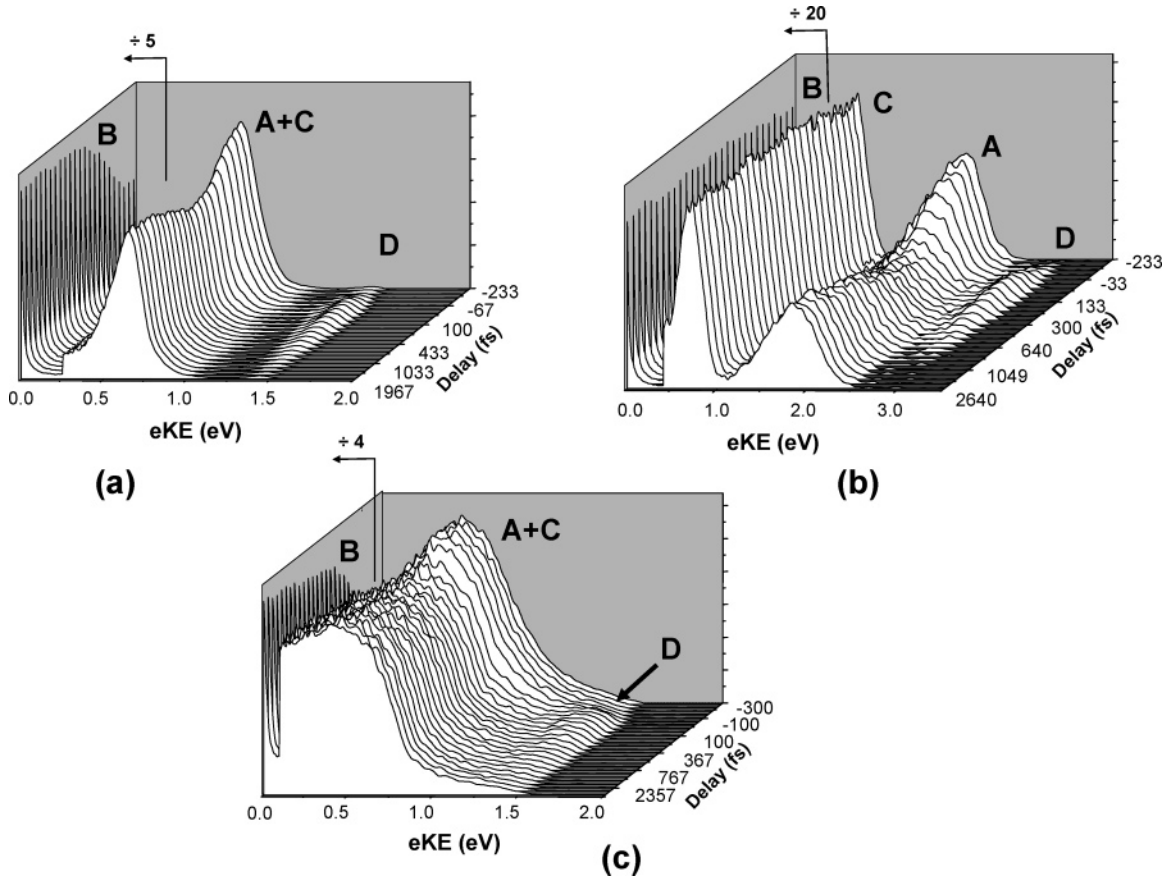

Figure 5. Spectral waterfall plots of representative $(D_2O)_n^-$ relaxation dynamics for both isomers: (a) $(D_2O)_{15,I}^-$; (b) $(D_2O)_{25,I}^-$; (c) $(D_2O)_{80,II}^-$. For (a) and (c), $\lambda_{pump} = 1650$ nm, $\lambda_{probe} = 790$ nm. For (b), $\lambda_{pump} = 1250$ nm, $\lambda_{probe} = 395$ nm. Pump−probe delays are indicated, with spectral contributions labeled according to processes presented in Figure 2b.

overlapping detachment contributions in each spectral window (cf. Figure 3 and Figure 5a, where direct detachment from isomer III overlaps the [1+1′] signal), A_2 is the amplitude of the time-evolving two-color signal, and τ is the relaxation lifetime. This function is flexible for fitting the temporal characteristics of all features observed; curves obtained from these fits are superimposed on the integrated intensities in Figure 6.

Fits to features D and A, with positive and negative A_2, respectively, to account for signal increase and depletion, yield decay/recovery lifetimes τ of 463 ± 60, 398 ± 50, and 445 ± 41 fs for $(D_2O)_{15,I}^-$, $(D_2O)_{25,I}^-$, and $(D_2O)_{80,I}^-$, respectively, for the pump−probe schemes highlighted in Figures 3−6. Feature B, the lowest-*eKE* feature, could be modeled by a step function for $(D_2O)_{25,I}^-$ and all larger isomer I clusters. In contrast, the fit is improved for small $(D_2O)_{n,I}^-$ and large $(D_2O)_{n,II}^-$ by including a residual single-exponential component that increases with the same time constant τ used to fit features "A + C" and D. The origin of this residual exponential is considered below.

Figure 7 highlights the size and isotopomer dependence of the cluster electronic relaxation dynamics. The relaxation of isomer I [Figure 7a] exhibits both a marked size and isotopomer dependence across the investigated size range ($13 < n < 100$). The relaxation lifetime decreases from 463 ± 60 fs to 276 ± 23 fs from $(D_2O)_{15,I}^-$ to $(D_2O)_{35,I}^-$ and from 276 ± 23 fs to 154 ± 15 fs from $(D_2O)_{35,I}^-$ to $(H_2O)_{35,I}^-$. On the other hand, while the electronic relaxation of isomer II exhibits a clear isotopomer dependence ($\tau_H/\tau_D \sim 2$), it shows no obvious size dependence. This is illustrated in Figure 7b, in which normalized time-dependent, two-color (i.e., feature D) decay traces for all isomer II clusters studied ($n = 60$, 70, 80, 90, 100) have been overlaid.

Measured decay lifetimes for all sizes, both isotopomers, and both isomers are plotted against $1/n$ in Figure 8. This plot builds from our preliminary reports,[30,45] including isomer I electronic-decay lifetimes for an extended size range. As noted previously,[45] decay lifetimes of larger isomer I clusters ($n \geq 25$) extrapolate linearly with $1/n$ to an ultrafast (50 fs) *p*-to-*s* internal conversion of the bulk-hydrated electron; the origin of this dependence is not completely understood, as discussed further in section 5. Linear regression of excited-state lifetimes in this size regime against $1/n$ (dotted lines) yields a bulk-hydrated electron relaxation lifetime of 54 ± 30 (72 ± 22) fs in H_2O (D_2O), in excellent agreement with the 50-fs (70-fs) internal conversion lifetime reported by Pshenichnikov et al.[12] (plotted at $1/n = 0$). Lifetimes obtained for larger $(D_2O)_{n,I}^-$ clusters ($n =$ 50, 70, 100) through 790 nm + 395 nm pump−probe imaging match this trend, supporting the noted extrapolation. Importantly, decay lifetimes measured using 1250 and 790 nm pump pulses at large sizes ($n = 45$, 50) match within error, as do lifetimes measured using both the 1650 and 1250 nm pump wavelength at smaller cluster sizes ($n = 25$, 28, 30). The gradient in the size dependence of the isomer I electronic relaxation lifetimes changes abruptly in a range of 20−25 water molecules; this size-critical behavior is indicated by the vertical dashed line in Figure 8, with more weakly size-dependent decay lifetimes

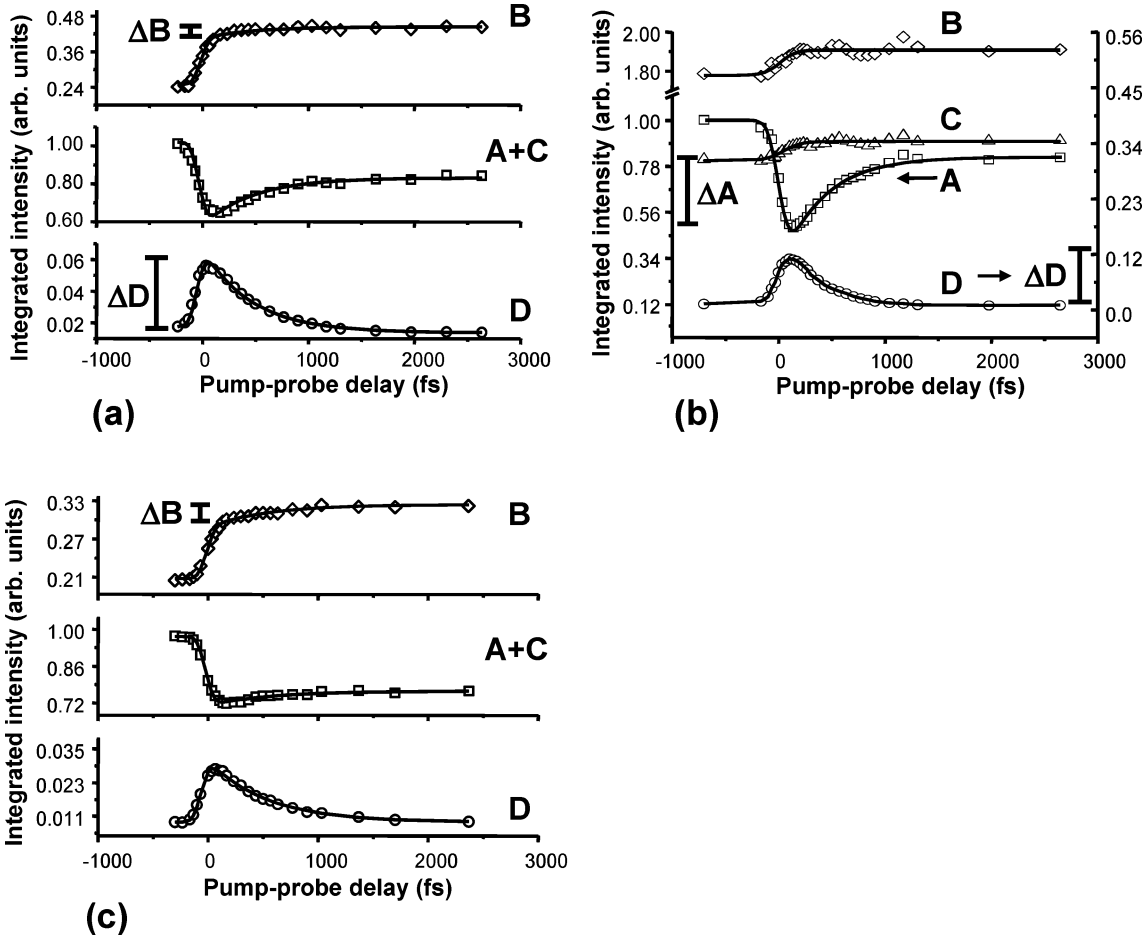

Figure 6. Time-resolved detachment dynamics of water cluster anions: (a) $(D_2O)^-_{15,I}$; (b) $(D_2O)^-_{25,I}$; (c) $(D_2O)^-_{80,II}$. Dynamics have been assessed according to the time-evolving integrated intensity of various spectral components, labeled according to the processes outlined in Figure 2b. Fits to the integrated intensities (black lines) are described in section 4.1. Δ"X" refers to the time-dependent signal amplitude of a feature "X" at positive delay times. Note expanded vertical axis (left) for feature D in (b).

measured at smaller sizes. The relaxation lifetimes of large isomer II clusters range from 450 to 520 fs for $(D_2O)^-_{n,II}$ and from 200 and 250 fs for $(H_2O)^-_{n,II}$, but these variations lie within the error bars of the measurement.

4.2. Photoelectron Angular Distributions. Photoelectron angular distributions (PADs) are intimately related to the shape of the electronic orbital from which a photoelectron originates.[59] The PAD at kinetic energy ϵ, $I(\theta,\epsilon)$, generated through an n-photon process with parallel, linearly polarized laser pulses is given by

$$I(\theta,\epsilon) \propto \frac{\sigma}{4\pi}[1 + \sum_{i=1}^{n}\beta_{2i}(\epsilon)P_{2i}(\cos\theta)] \qquad (2)$$

in which σ is the total photodetachment cross-section, $P_m(\cos\theta)$ is the mth-order Legendre Polynomial, and $\beta_m(\epsilon)$ is the mth-order, energy-dependent anisotropy moment of the photoelectron distribution. Hence, β_2 specifies the PAD for a one-photon process, while β_2 and β_4 are required for a two-photon PAD. These parameters have been determined for direct one- and resonant two-photon detachment distributions measured from $(H_2O)^-_n/(D_2O)^-_n$ at various sizes, both isomers, and various excitation wavelengths using the pBASEX forward-convolution image reconstruction method recently developed by Garcia et al.[60] This method uses a set of radial 3D basis functions, such that the radius(energy)-dependent anisotropy parameters are directly extracted from the expansion coefficients. The center-line noise found in images reconstructed using ordinary BASEX is eliminated in pBASEX, resulting in a more precise determination of positive anisotropy moments (for which intensity is maximal along the center line of the image).

Figure 9a−c show the results of this analysis. All extracted anisotropy parameters were positive. Anisotropy parameters for the direct 395 nm and resonant 790 nm photodetachment of isomer I clusters are plotted in Figure 9a; the estimated error shown applies to all values. Results at 790 nm are reported only for clusters with $n \geq 28$; there is essentially no two-photon signal for smaller clusters since one-photon detachment dominates. Anisotropy parameters for direct 395, direct 790, and resonant 1650 nm detachment of large isomer II clusters are plotted in Figure 9b. The β_2 parameter measured here at 395 nm for $(H_2O)^-_{18,I}$ (0.77 ± 0.12) is close to the value measured by Johnson at 532 nm (0.92 ± 0.1).[62] The PAD moments in these two plots do not change appreciably with the cluster size or detachment scheme for either isomer. The β_2 parameters for isomer I clusters in Figure 9a indicate considerably more anisotropic PADs for one photon detachment at 395 nm than for two-photon detachment at 790 nm. This trend is not seen

(62) Campagnola, P. J.; Posey, L. A.; Johnson, M. A. *J. Chem. Phys.* **1990**, *92*, 3243.

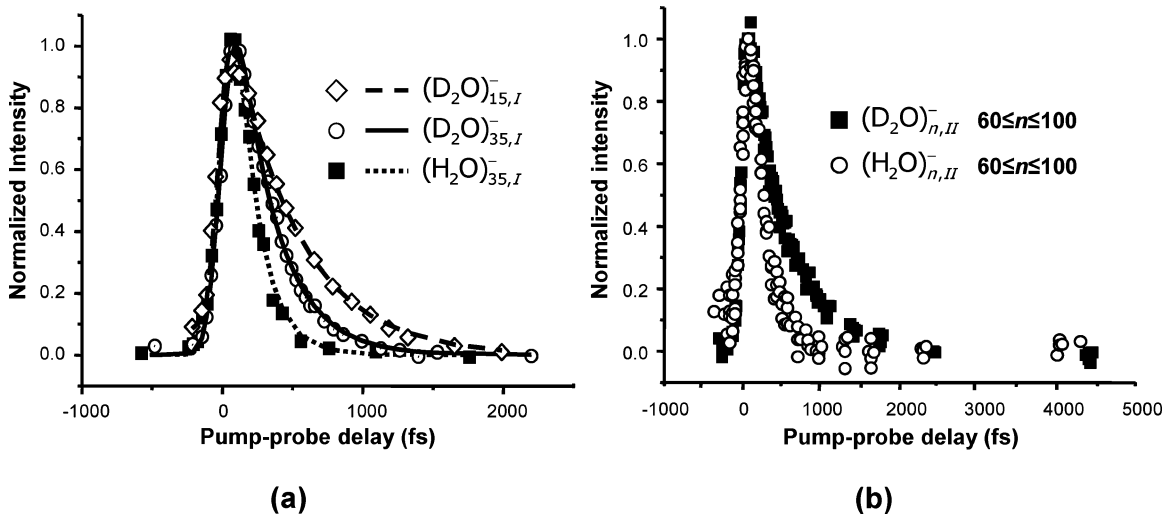

Figure 7. Comparison of size- and isomer-dependent electronic decay traces. (a) $(D_2O)^-_{n,I}$ and $(H_2O)^-_{n,I}$; normalized, time-dependent integrated intensities (symbols) and fits (lines) for various sizes have been plotted. (b) $(D_2O)^-_{n,II}$ and $(H_2O)^-_{n,II}$; normalized, time-dependent integrated intensities for all cluster sizes investigated have been overlaid.

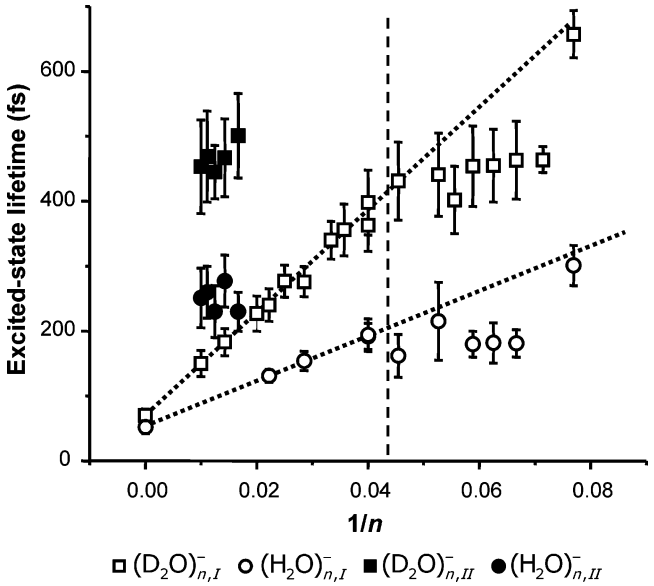

Figure 8. Size-, isotopomer-, and isomer-dependent excited-state electronic lifetime trends of water cluster anions. Lifetimes are plotted against $1/n$. Bulk lifetimes ($1/n = 0$) were taken from ref 12. Dotted lines, added to guide the eye, demonstrate the linear $1/n$ extrapolation of cluster IC lifetimes to the bulk for $n \geq 25$. Trends are discussed in section 5.

for isomer II, where β_2 for two-photon detachment at 1650 nm is about the same as for one-photon detachment at 790 nm and larger than that at 395 nm.

Figure 9c plots the anisotropy parameters derived from resonant 1650 and 1250 nm detachment distributions of small isomer I clusters. While the parameter values obtained from 1250 nm R2PD distributions are relatively constant, as at 790 nm, the magnitude of the β_2 and β_4 values determined from 1650 nm R2PD PADs switch at $n = 20$; this difference is seen clearly in the PADs collected from clusters at each end of this size range [Figure 9d].

5. Discussion

Numerous electronic and nuclear relaxation processes can occur following the excitation of an excess electron in a water cluster, many of which are outlined schematically in Figure 10. As has been suggested for the bulk-hydrated system,[7,63] excited-state solvation dynamics might occur following cluster excitation, such that the solvent adjusts to accommodate and stabilize the excited-state charge distribution. The excited state, "*p*"-$(H_2O)^-_n$, may decay electronically through internal conversion (IC) or via excited-state autodetachment (ESAD), since the excited state lies above the cluster adiabatic binding energy. Clusters that have relaxed via IC, "*s*"-$(H_2O)^{-\dagger}_n$, are anticipated to be highly vibrationally excited (†) and may undergo fragmentation, ground-state autodetachment (GSAD), or isomerization. In the sections below, we demonstrate how time-resolved PE spectra may be used to decipher the complex relaxation that follows electronic excitation, and how these pathways vary with cluster size and isomer.

5.1. Competition between Internal Conversion and Autodetachment. The time-dependent features in Figures 5 and 6, assigned in reference to Figure 2b, allow one to track state populations and relaxation pathways in considerable detail. Near $t = 0$, the abrupt drop in feature A and concomitant abrupt increase in features B and D occur as the pump pulse transfers electronic population to the excited state of the cluster. The subsequent recovery of A and drop in D, both of which occur over the same time constant τ in eq 1, reflect the presence of a direct electronic relaxation pathway back to the ground state via $p \rightarrow s$ internal conversion.

While τ represents the excited-state lifetime, it only represents the IC lifetime if no parallel processes, particularly ESAD, contribute significantly to the total relaxation mechanism. The partial recovery of feature A, probe-induced detachment from the ground state, might at first appear to indicate that not all the excited-state population relaxes to the ground state. However, this partial recovery also reflects depletion of the ground-state population by pump-induced detachment processes, such that feature A will always be more intense when the probe pulse comes before the pump pulse (i.e., $t < 0$).

Feature B provides a clearer indication of whether parallel excited-state relaxation processes are operative. It arises from pump-induced direct detachment *and* from any autodetachment

(63) Thaller, A.; Laenen, R.; Laubereau, A. *Chem. Phys. Lett.* **2004**, *398*, 459.

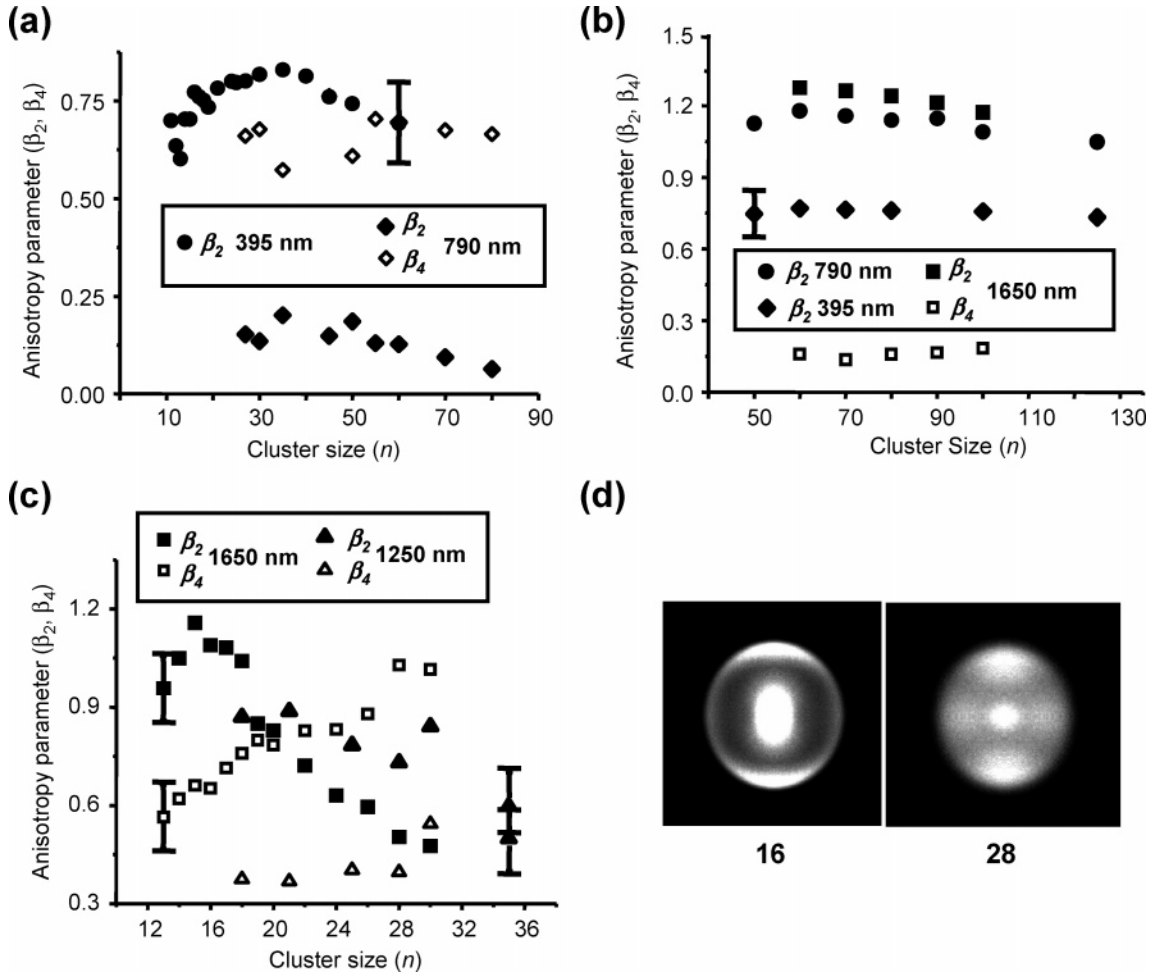

Figure 9. Size-dependent anisotropy parameters β_2 and β_4 characterizing photoelectron angular distributions (PADs) collected with direct and two-photon resonant detachment schemes for both isomers and at various cluster sizes. Isomers and excitation schemes: (a) (isomer I) 395 nm direct and 790 nm resonant; (b) (isomer II) 395 and 790 nm direct, 1650 nm resonant; (c) (isomer I) 1650 and 1250 nm resonant. (d) Images collected at each end of the small isomer I regime [see part c] through resonant detachment at 1650 nm. Anisotropy values are determined as described in section 4.2.

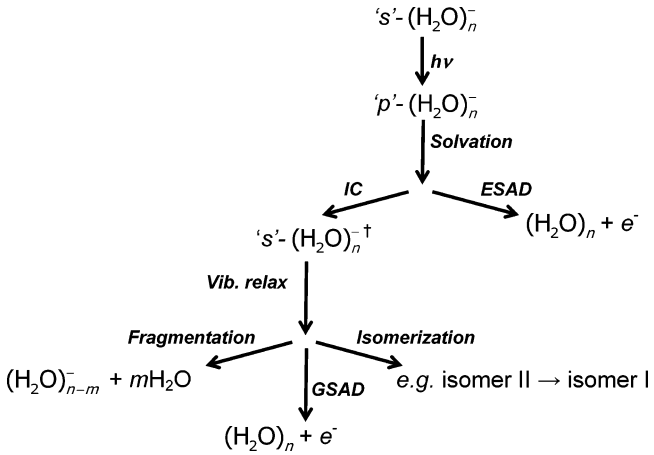

Figure 10. Pictorial representation of possible relaxation dynamics in water cluster anions following electronic excitation. "*p*" and "*s*" refer to the excited and ground electronic states, respectively. Possible electronic decay pathways include internal conversion (IC) and excited-state autodetachment (ESAD). Vibrational/nuclear relaxation dynamics in the ground state may include vibrational relaxation, fragmentation, isomerization, and ground-state autodetachment (GSAD).

(ESAD or GSAD) that might occur from those ions that have absorbed only a single pump photon. In particular, ESAD is reflected by the increase in this feature, ΔB in Figure 6, that occurs with the same time constant τ as the excited-state lifetime. At delay times $0 < t \ll \tau$, ESAD is shut off by probe-induced depletion of the excited-state population, while, for $t \gg \tau$, the excited-state population is fully decayed. The magnitude ΔB is thus a relative measure of excited-state decay by autodetachment versus internal conversion. For isomer I clusters with $n \geq 25$, we find $\Delta B = 0$, indicating ESAD to be negligible, such that $\tau = \tau_{IC}$, as claimed previously.[45] However, $\Delta B \neq 0$ for smaller isomer I clusters and for all isomer II clusters, indicating that ESAD and IC are competitive processes in the relaxation mechanism of these clusters.

Quantitatively, if we define $\Delta B(t)$ as the ESAD signal at pump−probe delay t relative to that at $t = 0$, then

$$\Delta B(t) \propto \frac{k_{AD}}{k_{AD} + k_{IC}} \cdot ES^{(0)} \cdot \sigma_{pr} \cdot \phi \cdot (1 - e^{-t/\tau}) \qquad (3)$$

where k_{AD} and k_{IC} are the ESAD and IC rate constants, $ES^{(0)}$ is the initial excited-state population created by the pump pulse, σ_{pr} is the photodetachment cross-section of the excited state at the probe laser wavelength, and ϕ is the probe laser flux. As $t \rightarrow \infty$, $\Delta B(t) \rightarrow \Delta B = \{k_{AD}/(k_{AD} + k_{IC})\} \cdot ES^{(0)} \cdot \sigma_{pr} \cdot \phi$, while ΔD is given by $ES^{(0)} \cdot \sigma_{pr} \cdot \phi$. Hence,

$$\Delta B/\Delta D = \frac{k_{AD}}{k_{AD} + k_{IC}} \equiv \phi_{AD} \quad (4)$$

In $(D_2O)^-_{15,I}$ [Figure 6a], for instance, the ratio $\Delta B/\Delta D$ is roughly 1/3.5. Consequently, while the overall lifetime τ is 463 fs, the IC and ESAD lifetimes are ~650 and ~1600 fs, respectively. Equation 4 is a measure of the autodetachment quantum yield, ϕ_{AD}. For $n = 15$, $\phi_{AD} \approx 0.3$ but drops to 0 for $n \geq 25$. These measurements provide new information on the asymptotic decay channels of electronically excited water clusters that complement previous measurements of the photofragmentation quantum yield, ϕ_F, by Johnson and co-workers.[64,65] The autodetachment channel has the effect of lowering the overall electronic relaxation lifetime relative to the IC lifetime, as the parallel decay rates are additive. We believe the presence of excited-state autodetachment accounts for the difference between the two dynamical regimes observed for isomer I, specifically the deviation of the lifetimes below $n = 25$ from the $1/n$ dependence in Figure 8.

For large isomer II clusters, such as $(D_2O)^-_{80,II}$ [Figure 6b], ϕ_{AD} is quite substantial (~0.5), implying that ESAD is at least as important as IC and may be the dominant decay mechanism. The recovery of feature A + C in Figure 6c shows that some internal conversion occurs, but the amplitude of this recovery is considerably smaller than that for the isomer I clusters in Figure 6a and b; this observation is also consistent with substantial ESAD for the isomer II clusters.

It is difficult to precisely determine the ESAD vs IC rates because the relatively small changes to feature B occur on top of a large background. This situation is exacerbated for isomer II clusters, for which there is a significant overlap of features B and D with feature A + C [Figure 4c]; for this reason only the integrated intensity of the high-energy half of D is plotted in Figure 6c. Nonetheless, the qualitative trends extracted from the above analysis appear to be valid. While IC is the dominant excited-state relaxation pathway for isomer I clusters, and the only pathway for isomer I clusters with $n \geq 25$, ESAD is considerably more important for isomer II clusters. Furthermore, isomer I clusters with $13 \leq n \leq 25$ represent a transitional regime in which autodetachment becomes progressively less important.

The identification of ESAD as a decay channel represents a significant, additional probe of the nature of the excess electron in water cluster anions. As discussed in section I, isomer I and isomer II clusters have been assigned previously to species with internalized and surface-bound electrons, respectively. The observations that IC is the only channel for isomer I clusters with $n \geq 25$ while ESAD is a major channel for isomer II clusters are consistent with such an assignment, since autodetachment should be more facile if the electron is localized on the surface of the cluster. However, the isomer I results for $13 \leq n \leq 25$ suggest a refinement of this picture, in which this size range of clusters represents a transitional regime where the excess electron becomes progressively more internalized. The issue of surface vs internalized states is discussed further in section 5.5.

5.2. Other Dynamical Processes. For all clusters studied here, the excited-state feature (D) decays with no appreciable shift in its shape or average kinetic energy, indicating that significant excited-state solvation dynamics do not occur prior to internal conversion or that excited-state solvent rearrangement does not alter the photodetachment Franck−Condon profile. In contrast, as reported by Paik et al.[46] the ground-state feature (A) recovers with a time-decaying tail at high *eKE*, indicating a relaxation of excess vibrational excitation in the ground state on a ~400-fs time scale following the internal conversion process. The absence of observable excited-state solvation is consistent with the findings of mixed quantum-classical MD simulations of the excited electron in bulk water presented by Schwartz and Rossky.[16] In these simulations, the occupied *p*-state exhibits no shift in its energy with time, though the unoccupied *s* and the other unoccupied *p*-states destabilize with the time-dependent solvent response following $p \leftarrow s$ excitation. Consequently, while transient absorption experiments of the excited electron in the bulk may be sensitive to the appearance of new $p' \leftarrow p$ resonances, the photodetachment experiment is only sensitive to the "free electron" $\leftarrow p$ process, which is not sensitive to the solvent response. The absence of observable excited-state solvation in our studies is therefore consistent with the "adiabatic" MD simulations as well as the "nonadiabatic" relaxation mechanism but contrasts with kinetic models, loosely based on MD simulations, that have included an energetically stabilized, solvated *p*-state in the electronic relaxation pathway of the bulk-hydrated electron.[63]

Other ground-state processes, in addition to ground-state solvation, should also be observable in the time-resolved photoelectron spectra. For instance, as was demonstrated in recent studies of Hg_n^- anions,[66,67] fragmentation will produce daughter ions with lower VBEs than those of the parent cluster. Ground-state autodetachment (GSAD) should manifest itself as a long-time increase in low-energy photoelectrons with a concomitant decrease in a ground-state detachment signal with increased pump−probe delay; this process should occur in a manner similar to ESAD, whereby GSAD intensity is shut off at early times as electrons are probed from the ground electronic state. We do not see evidence for either fragmentation or GSAD on the time scales probed in our experiments (i.e., 5−20 ps).

We also searched for isomerization of isomer II clusters after electronic excitation and internal conversion, speculating that the surface electron might migrate to the interior of the vibrationally excited cluster, dramatically increasing the cluster VBE. Surface-to-interior electron migration dynamics have been predicted to occur on a ~2 ps time scale in warm (300 K) water clusters,[35] warranting investigation of this possibility. However, time-resolved data obtained from isomer II employing a 1650 nm + 395 nm pump−probe scheme showed no clear detachment signature of isomer I at long times (~600 ps). This result may indicate that the clusters that do relax by internal conversion do not have enough internal energy to climb over whatever barriers exist for isomerization or that perhaps the prominence of ESAD in isomer II clusters makes it much more difficult to observe this process experimentally, since those cluster anions that autodetach cannot convert to isomer I.

As demonstrated above, the integrated intensities of time-dependent features reflect the population-transfer dynamics

(64) Posey, L. A.; Campagnola, P. J.; Johnson, M. A.; Lee, G. H.; Eaton, J. G.; Bowen, K. H. *J. Chem. Phys.* **1989**, *91*, 6536.
(65) Posey, L. A.; Johnson, M. A. *J. Chem. Phys.* **1988**, *89*, 4807.
(66) Bragg, A. E.; Verlet, J. R. R.; Kammrath, A.; Cheshnovsky, O.; Neumark, D. M. *J. Chem. Phys.* **2005**, *122*, 054314.
(67) Verlet, J. R. R.; Bragg, A. E.; Kammrath, A.; Cheshnovsky, O.; Neumark, D. M. *J. Chem. Phys.* **2004**, *121*, 10015.

between states and the detachment cross-sections of the ground and excited electronic levels. Consequently, for clusters in which IC is the only excited-state relaxation pathway (i.e., isomer I, $n \geq 25$), the relative cross-sections of the excited and ground states may be assessed from the temporal intensity traces plotted in Figure 6. In particular, the ratio $\Delta A/\Delta D$ gives the relative cross-sections of the ground and excited states at the probe wavelength. In $(D_2O)^-_{25,I}$ [Figure 6b] this ratio is ~4, indicating that the ground-state photodetachment cross-section is roughly 4 times that of the excited state. Examination of all larger isomer I time-dependent signal traces (H_2O and D_2O) gives an average ratio of 3 ± 1.

5.3. Photoelectron Angular Distributions. The photoelectron angular distributions offer an additional, if indirect, probe of electronic structure in these clusters, in particular the nature of the ground- and excited-state orbital from which the excess electron is ejected. For atomic systems,[68] photodetachment from an *s*-orbital near threshold results in ejection of a *p*-wave ($\beta_2 = 2$), while a *p*-orbital detaches to an *s*-wave ($\beta_2 = 0$). This trend is in qualitative agreement with the anisotropy parameters in Figure 9a, where $\beta_2 \cong 0.75$ for one photon detachment of isomer I clusters at 395 nm and is much smaller, around 0.12, for resonant two-photon detachment at 790 nm (for clusters with $n \geq 28$, see section 4.2). These results are consistent with assignment of the ground and excited states of these clusters as "*s*" and "*p*" states. This trend is not seen in Figure 9b for isomer II clusters, where resonant two-photon detachment at 1650 nm and direct detachment at 790 nm have similar β_2 parameters, around 1.2, for clusters comprising 50−130 water molecules. This result suggests that the shape of the excited-state wave function is quite different in the isomer II and larger isomer I clusters.

The only size-dependent trend in the PADs appears in Figure 9c, where β_2 for small isomer I clusters from resonant two-photon detachment at 1650 nm drops from ~1.2 to 0.4 as *n* increases from 13 to 30, while the β_4 parameters increase over the same size range. The β_2 values for the smallest isomer I clusters are similar to those for two-photon detachment of isomer II clusters at the same wavelength, while the loss of anisotropy with increasing *n* leads to β_2 values similar to (but slightly larger than) those for the larger isomer I clusters (two-photon, 790 nm) in Figure 9a. This trend, along with the autodetachment results discussed in section 5.1, provides additional evidence for small isomer I clusters representing a transitional regime between experimental observables associated with isomer II and larger isomer I clusters.

5.4. Size-Dependent Characteristics of Isomer I Water Cluster Anions. The results in Figures 2a and 8 for isomer I cluster anions show that the VBEs for $n = 11-125$ lie on a straight line when plotted as a function of $n^{-1/3}$. In contrast, the excited-state lifetimes τ for $n \geq 25$ decrease linearly as a function of $1/n$ for $(H_2O)^-_n$ and $(D_2O)^-_n$, extrapolating smoothly to the IC lifetimes for e^-_{aq} assigned by Wiersma and co-workers.[12]

For isomer I clusters with $n \geq 25$, the $1/n$ size dependence of the IC lifetimes is quite different from the trend in VBEs, for which the size dependence is well-described according to a simple electrostatic model,[25,26] scaling with the characteristic $1/R$ ($n^{-1/3}$) radial dependence of a spherically symmetric potential. The IC rates are also clearly not scaling as the density of vibrational states of the solvent molecules, as might be expected from Fermi's Golden Rule, because this density would rise far more quickly than *n*. In their studies of hydrated-electron dynamics in the bulk, Pshenichnikov et al.[12] invoked a conical intersection (CI) mediated by local OH(OD) stretch vibrations to explain a 50(70)-fs internal conversion of the excited hydrated electron. If this is a proper explanation of the nonadiabatic process, the lifetime size dependence of large isomer I clusters likely derives from a size-dependent perturbation of a CI between the *p* and *s* states of the excess electron and may be amenable to the general formalism recently developed by Cederbaum et al.[69] to treat CI dynamics in the presence of a large number of bath modes. Alternatively, mixed quantum-classical simulations on water cluster anions, of the type used previously on the bulk hydrated electron,[16,17,19,20,70,71] may provide further insight into the size-dependent dynamics seen in our experiment. Such calculations are currently being carried out by Rossky and co-workers.[72]

5.5. Dynamics of Hydrated Electrons: From Clusters to Bulk. Despite the copious attention the equilibrated hydrated electron, e_{aq}^-, has received, it has been challenging to elucidate the mechanism by which this species relaxes to equilibrium following electronic excitation in aqueous solution. In time-resolved experiments, the ensemble dynamics of a solvated electron are generally tracked according to the time-, wavelength-, and polarization-resolved transient absorption signal of the electron in its prepared and nascent relaxing states.[7,8,12,17,73] These signals arise from a combination of largely overlapping induced absorption, stimulated emission, and absorption bleach components, such that fits to various nonunique kinetic relaxation models have been attempted to explain the dynamics that occur on three distinct time scales with time constants on the order of 50 fs, 200−300 fs, and 1 ps.[7] A key issue in the interpretation of the transient absorption experiments has been whether the intermediate time constant corresponds to the $p \rightarrow s$ internal conversion lifetime (adiabatic solvation model[17]) or to relaxation of the nascent, unequilibrated *s*-state formed by internal conversion on a 50-fs time scale (nonadiabatic solvation).[6,7,12] This issue has also been explored through time-resolved resonance Raman studies[11,74] and time-resolved electron scavenging experiments[75] of the hydrated electron in various electronic states and precursor states. While more experiments have been analyzed in terms of the longer rather than shorter IC lifetime, some of the more extensive recent work has noted that this issue is still unresolved.[7,76]

In contrast to the bulk environment, pathways for electronic relaxation dynamics are readily identified in experiments on water cluster anions. Our experiments have demonstrated clear signatures of direct $p \rightarrow s$ decay in $(H_2O)^-_{n,I}/(D_2O)^-_{n,I}$ ($25 \leq n \leq 100$). This relaxation process is characterized by the direct decay

(68) Cooper, J.; Zare, R. N. *J. Chem. Phys.* **1968**, *48*, 942.
(69) Cederbaum, L. S.; Gindensperger, E.; Burghardt, I. *Phys. Rev. Lett.* **2005**, *94*.
(70) Schwartz, B. J.; Rossky, P. J. *J. Chem. Phys.* **1996**, *105*, 6997.
(71) Schwartz, B. J.; Rossky, P. J. *J. Phys. Chem.* **1994**, *98*, 4489.
(72) Rossky, P. J. Private communication.
(73) Cavanagh, M. C.; Martini, I. B.; Schwartz, B. J. *Chem. Phys. Lett.* **2004**, *396*, 359.
(74) Mizuno, M.; Yamaguchi, S.; Tahara, T. *J. Phys. Chem. A* **2005**, *109*, 5257.
(75) Kee, T. W.; Son, D. H.; Kambhampati, P.; Barbara, P. F. *J. Phys. Chem. A* **2001**, *105*, 8434.
(76) Kambhampati, P.; Son, D. H.; Kee, T. W.; Barbara, P. F. *J. Phys. Chem. A* **2002**, *106*, 2374.

of the excited electronic state with concomitant repopulation of the electronic ground state at these sizes, but with parallel excited-state autodetachment at smaller sizes. As discussed previously,[45] the observed rapid relaxation lifetimes, dynamical isotope effect, absence of observable upper-state solvation dynamics, and extrapolation of cluster lifetimes to ultrafast bulk IC lifetimes of 50 fs in H_2O and 70 fs in D_2O are consistent with the "nonadiabatic" relaxation mechanism of the bulk hydrated electron.[6,12] According to this mechanism, IC occurs first on a 50 fs time scale followed by a two-step ground-state relaxation process on the longer ~300 fs and ~1 ps time scales that have been measured in transient absorption experiments. These latter time scales match well with experimental work by Paik et al.,[46] who found biexponential ground-state relaxation in cluster anions ($15 < n < 35$) with time scales of 380 ± 150 fs and 2−10 ps, respectively, following internal conversion. Overall, the cluster anion dynamics experiments[45,46] support assignment of the time scales measured in the bulk experiment to steps of a nonadiabatic relaxation model.

The extrapolation of cluster properties to those of e_{aq}^- assumes that the excess electron in the clusters bears some resemblance to that in the bulk, an assumption that is easier to justify if the electron is internalized in the cluster anions. Our assignment of isomers I and II to internalized and surface-localized states was based primarily on trends in vertical binding energies and supported by trends in excited-state lifetimes vs size for the two isomers.[30] This assignment is consistent with the competition discussed in section 5.1 between excited-state autodetachment and internal conversion in isomer I and isomer II clusters, with the caveat that isomer I clusters with $n < 25$ appear to lie in a transitional regime. While these energetic and dynamical trends are compelling, in our view, they do not represent structural probes of the water cluster anions, and one must view the issue of internal vs surface solvation in these clusters as still amenable to both experiment and theory. Recent infrared spectroscopy experiments by Johnson and co-workers,[77] which show evidence for the excess electron binding to a double-acceptor water molecule for isomer I clusters as large as $n = 25$, should prove extremely valuable in this regard.

(77) Johnson, M. A. Private communication.
(78) Turi, L.; Sheu, W.-S.; Rossky, P. J. *Science* **2005**, *309*, 914.

On the theoretical side, Rossky and co-workers,[78] applying mixed quantum-classical MD methods to the simulation of water cluster ions, recently concluded that the energetic and spectral characteristics of isomer I clusters are consistent with a surface-bound binding motif. However, the VBE trends recovered from these simulations do not appear to rule out the association of isomer I with an internalizing/internally-solvated electron, since the absolute VBEs determined for surface-states in these simulations are very close to the experimental values found for isomer II. It will be of considerable interest to see if calculated excited-state lifetimes in these simulated clusters reproduce the trends for isomer I and II clusters reported here and elsewhere.[30,45,46]

6. Conclusions

The size-, isotopomer-, and isomer-dependent electronic relaxation dynamics of $(H_2O)_n^-/(D_2O)_n^-$ have been studied through time-resolved photoelectron imaging. In these experiments the excess electron was excited through the $p \leftarrow s$ transition, and its dynamics were probed temporally through photodetachment by time-resolved photoelectron imaging. Observed dynamics reflect $p \rightarrow s$ nonradiative decay for all sizes, isotopomers, and isomers studied. Measured lifetimes and lifetime size dependences for different electron localization modes and size regimes suggest the development of bulklike hydration properties in isomer I clusters as small as $n = 25$. In contrast, the electronic decay dynamics of small isomer I clusters and large isomer II clusters supporting surface-localized electrons reveal competition between internal conversion and excited-state autodetachment decay pathways. These findings offer renewed perspective on fundamental aspects of the dynamics of hydrated electrons.

Acknowledgment. This research is supported by the National Science Foundation under Grant No. CHE-0350585. Additional support from the U.S.−Israel Binational Science Foundation is gratefully acknowledged. A.E.B. would like to thank Dr. Ross Larsen for enlightening discussions about MD simulation methods.

JA052811E